The 2020 World Congress on
Advances in Civil, Environmental, & Materials Research (ACEM20)
25-28, August, 2020, GECE, Seoul, Korea

Dynamic calibration of accelerometer-based drag balance system

*Byungkook Jang[1)], Keunyeong Kim[2)], and Gisu Park[3)]

[1), 2), 3)] Department of Aerospace Engineering, KAIST, Daejeon 34141, Republic of Korea
[1)] bk_jang@kaist.ac.kr
[2)] scorpius_a@kaist.ac.kr
[3)] gisu82@kaist.ac.kr

ABSTRACT

In this study, dynamic calibrations of an accelerometer-based drag balance were performed to recover applied forces from measured acceleration signals. The system response function was determined using two types of force input. Impulse and ramp loads were applied to the system through impact hammer and known mass drop tests, respectively. Each calibration technique was validated by recovering the applied load using the dynamic response functions obtained from the other technique. The results showed that the recovered forces were in good agreement with the applied force inputs within the margin of error.

1. INTRODUCTION

Impulse facilities such as shock tunnels can be used to simulate hypersonic flow at lower costs, compared to other hypersonic facilities. However, owing to the operating characteristics of impulse facilities, very short test time up to the millisecond order is taken (Park et al. 2015~Park et al. 2008), which may restrict the force measurements. The conventional force measurement technique requires stabilization time for the strain gauge to achieve force equilibrium. However, it is difficult for an impulse facility to reach the stabilization time at the conventional force balance. Therefore, various force measurement techniques have been developed to overcome this problem, including the accelerometer-based force balance (Joshi and Reddy 1986). The accelerometer-based force balance is a technique in which a mounting system that allows the test model to move freely during a short test period is utilized. The acceleration of the model is measured using an accelerometer and converted to aerodynamic force. The mounting system has been fabricated using rubber bush (Satheesh and Jagadeesh 2009, Sahoo et al. 2003, Sahoo et al. 2007) or ball bearing (Joarder and Jagadeesh 2004) to minimize the restriction of free motion. Because of the minimum restriction exerted on the mounting system, it can be assumed that the damping effect is minimally influenced within the very

---

[1),2)] Graduate Student
[3)] Associate Professor, Corresponding Author

short test time in the shock tunnel. Hence, the measured acceleration can be directly converted to aerodynamic force using Newton's second law of motion. However, if a considerable restriction is exerted by the mounting system, which cannot be neglected, then the measured acceleration can be converted to aerodynamic force through the calibration of the balance. The calibration process includes determining the dynamic response characteristics of the system, which exists when an external force is applied. The determined system response characteristics are used to recover the system output (acceleration) back to system input (external force) using the inverse technique (Mee 2003).

In this study, the dynamic calibration of an accelerometer-based drag balance designed for drag measurement in a shock tunnel was performed. Two calibration techniques were applied to determine the system response functions of the force balance. The background of the calibration techniques is discussed in Section 3. Each calibration technique was validated by recovering the other type of load.

2. DRAG BALANCE SYSTEM

An accelerometer-based drag balance was designed to measure aerodynamic drag in a KAIST K1 shock tunnel for a short test time. The shock tunnel consisted of a shock tube, Mach 6 Nozzle, test section and dump tank. Detailed information regarding the shock tube can be found in Jo et al. 2019~Kim et al. 2019; the shock tunnel in Kim et al. 2017 and Lee et al. 2020. The drag balance had a weakly restrained support system to make the test model exhibit quasi-free flight along the axial direction. Fig. 1 shows a schematic of the balance system. The system consisted of a cone model (length of 36 mm and diameter of 24 mm), sting (length of 85 mm and diameter of 6 mm), accelerometer (length of 16 mm and diameter of 7 mm, Model 353B16, PCB Piezotronics), linear ball bush (inner diameter of 6 mm), and aerodynamic shield (outer diameter of 20 mm). The test model and sting were made of aluminum (Al-6061), which possessed adequate strength and weight, to improve the system response. The cone model and accelerometer were attached to the front and rear of the sting, respectively. The acceleration of the test model was recorded using an oscilloscope outside the test section connected to the accelerometer.

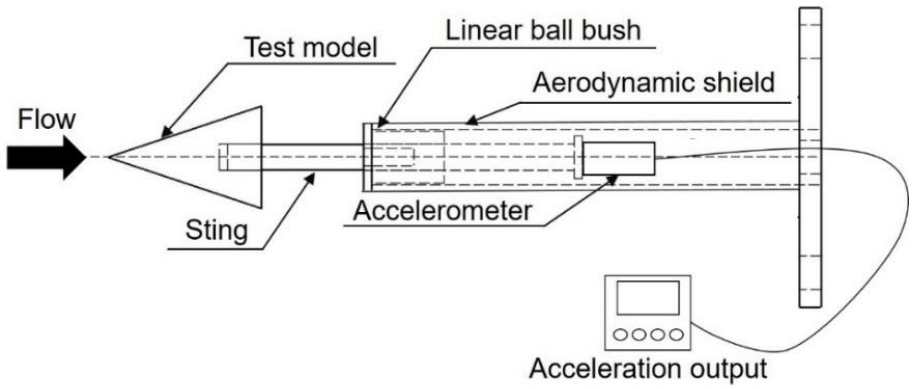

Fig. 1 Schematic of accelerometer-based drag balance system

3. DYNAMIC CALIBRATION

3.1 Balance calibration

When an aerodynamic load was applied on the drag balance during the shock tunnel tests, the model slid to the axial direction through the linear ball bush, and the model acceleration was measured. However, because of the frictional force acting between the sting and the linear ball bush, the measured acceleration history could not be directly converted to aerodynamic force history. Frictional forces can be included in the system response to aerodynamic forces. Therefore, the history of aerodynamic drag was determined by considering the dynamic response of the drag balance system. The process of converting acceleration to aerodynamic drag involved the system dynamic calibration process, which was used to derive the system response function. If the drag balance system is assumed to be a linear time-invariant system, the system response can be represented using the convolution integral (Prost and Goutte 1984, Satheesh and Jagadeesh 2009).

$$y(t) = \int_0^t g(t-\tau) f(\tau) d\tau \tag{1}$$

For the drag balance, f is the applied drag to the model, y is the measured acceleration of the model, and g is the system response function. If the system response function (system characteristics) is determined, the deconvolution method can be used to recover the applied aerodynamic drag history from the measured acceleration history. The system response function can be determined by applying a known force on the model and deconvolving the applied force and measured acceleration. Impulse and ramp-type forces were applied to obtain the system response function for the balance system. Next, the response functions of each calibration technique were validated by recovering another force input using system response functions determined from the other calibration technique.

3.2 Impact hammer

Impulse force was applied by tapping an impact hammer on the model (Model 086C01, PCB Piezotronics), which could record the impulse force history. The model arrangement and impact hammer are shown in Fig. 2(a). The impact hammer was equipped with a plastic tip, and no extender was used. The impulse force was measured using the piezoelectric element inside the hammer and recorded using an oscilloscope. The oscilloscope was triggered by the sudden change in the voltage signal from the impact hammer. Both the impulse force input and acceleration output were measured at 0.5 μs sampling period. Fig. 2(a) shows typical histories of the measured impulse hammer input and the acceleration output of the system. In the impulse force history, the force acting on the model should have been zero after the impulse force was applied, but weak electrical noise with high frequency was identified. The impulse force was approximately 0.46 ms and almost symmetrically shaped. The impulse force history showed a peak force of 62 N and rise time of 0.22 ms. In the acceleration output, a peak acceleration of 3742 m/s^2 and rise time of 0.16 ms were obtained. The impulse response function of the system can be obtained through numerical deconvolution of the impulse force input and acceleration output.

The impulse response function was validated by recovering the other type of force input. Fig. 2(b) shows the original ramp force input and recovered ramp force. The original force was generated by applying a known mass to the model (Fig. 3(a)). The recovered ramp force was obtained by deconvolving the measured acceleration using the impulse response function. The original and recovered ramp forces were within the margin of error for most ranges; however, the difference increased from 4.5 ms. This difference occurred because when an impulse response function was acquired, the impulse force history included electrical noise, which was nonzero values. Low electrical noise accumulated during the deconvolving process and caused a difference at the end of the recovered force. This difference could be reduced by eliminating electronic noise through filtering data.

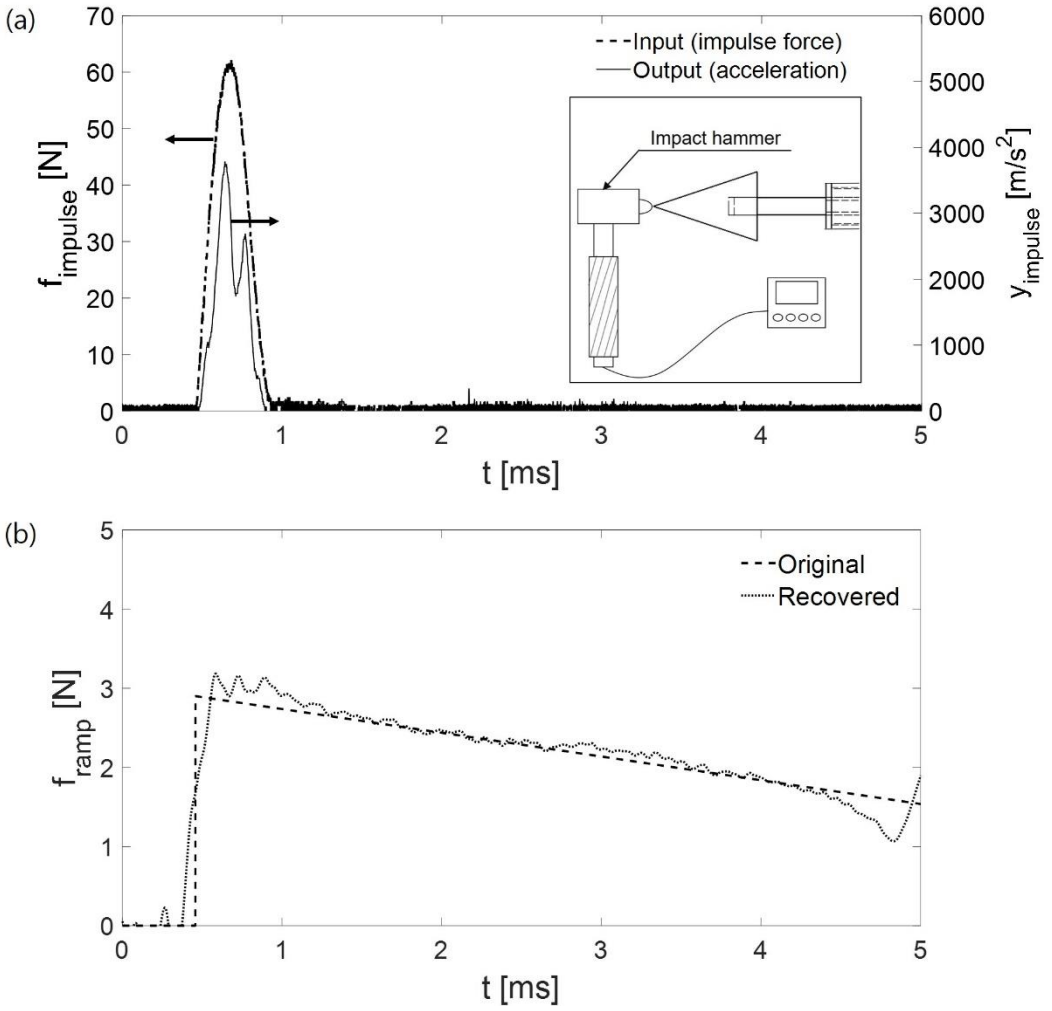

Fig. 2 Impact hammer test; (a) Impulse load calibration result; (b) Recovered ramp input using impulse response function

3.3 Dropping mass

The ramp force was applied by axially suspending the known mass from the model tip and cutting the wire attached to the model. The arrangements of the model and mass are shown in Fig. 3(a). The mass was attached to a pulley, which was used to apply the force axially. The maximum value of the ramp force was assumed to be equal to the weight of the mass. However, when the mass was dropped, frictional losses occurred as the pulley rotated. Therefore, the force input was determined by considering the loss. The oscilloscope was triggered based on the sudden change in the value of the voltage signal from the piezoelectric-based accelerometer. The acceleration output was measured at a 0.5 μs sampling period. Fig. 3(a) shows the assumed ramp force input and acceleration output of the system. The acceleration output history showed that the acceleration decreased gradually from 0.45 to 5 ms. The rate of decrease in the acceleration output was used to assume an applied force value. The rate of force loss was assumed to be proportional to the rate of decrease in acceleration. Therefore, the force applied during the calibration test was calculated as follows:

$$f_{ramp}(t) = Mg + f_{loss} = Mg + \left(\frac{Mg}{y_{ramp,max}}\right)\left(\frac{dy_{ramp}}{dt}\right)t \quad (2)$$

Where *M* is the mass, which is suspended to the model, *g* is the gravitational acceleration, f_{loss} is the loss in force generated by the pulley, y_{ramp} is the acceleration output of the ramp calibration test, and $y_{ramp,max}$ is the maximum acceleration in the first-order regression function of the acceleration history. The assumed ramp force had a maximum value of 2.9 N at an acceleration trigger point of 0.45 ms and gradually decreased to 1.54 N at 5 ms. The total number of applied force data was set equal to the acceleration output to carry out numerical deconvolution. The ramp response function can be obtained through numerical deconvolution of the ramp force input and acceleration output.

The ramp response function was validated by recovering the other type of force input. Fig. 3(b) shows the original impulse force input and recovered impulse force. The original force was generated by tapping the impact hammer on the model (Fig. 2(a)). The recovered impulse force was obtained by deconvolving the measured acceleration using the ramp response function. The original and recovered impulse forces were compared to validate the ramp response function acquired. A difference existed between both the original and recovered impulse forces within the margin of error.

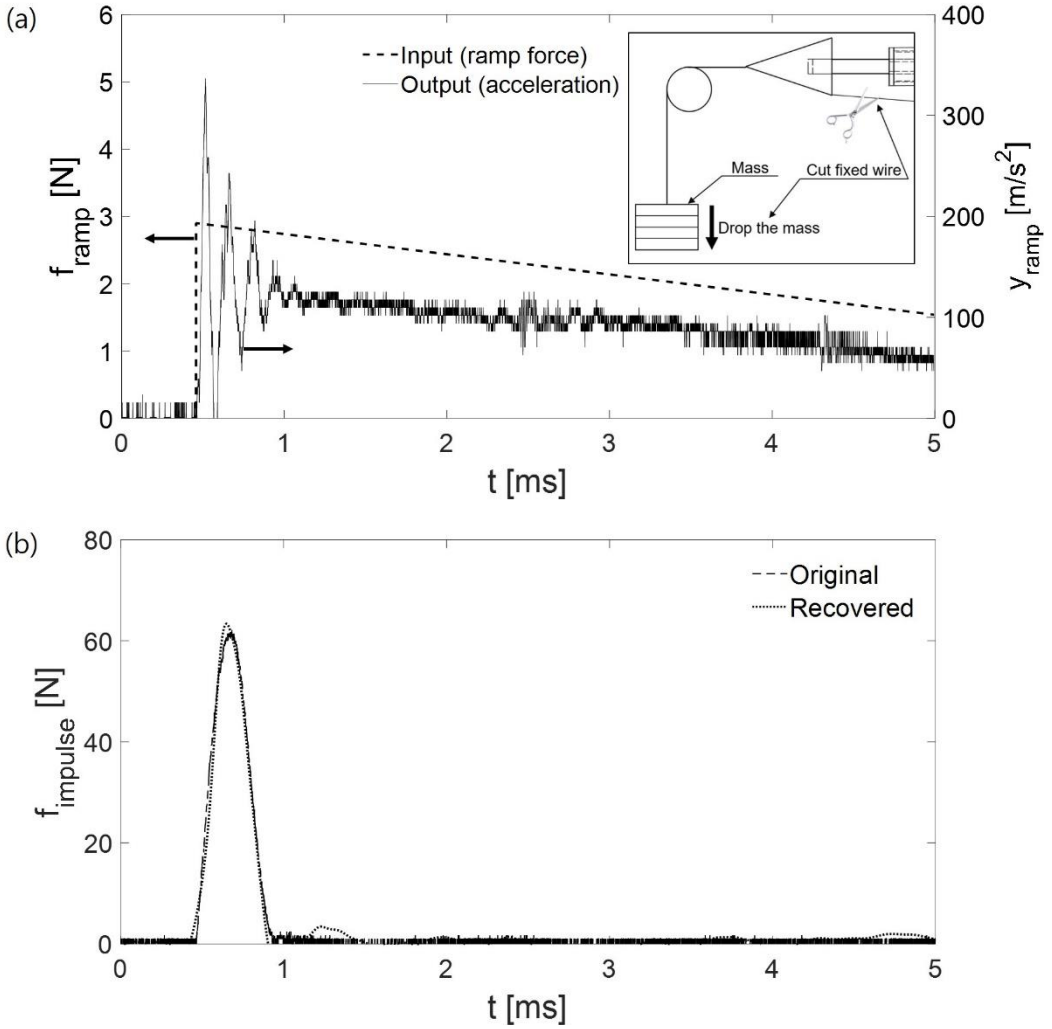

Fig. 3 Dropping mass test; (a) Ramp load calibration result; (b) Recovered impulse input using ramp response function

4. CONCLUSIONS

In this study, different techniques for performing the dynamic calibration of the accelerometer-based drag balance were applied. The dynamic calibration with impulse and ramp force inputs were conducted through impact hammer and dropping known mass tests, respectively. The response functions were validated by recovering the other known force inputs. The results showed that both calibration techniques were suitable for performing force measurement using the drag balance.

ACKNOWLEDGMENT

This work was supported by the Scramjet Combined Propulsion System Project (No. 16-106-501-035) of Republic of Korea.

REFERENCES

Park, G., Park, C., Jin, Y., Choi, H., Byun, J., and Hwang, K. (2015), "Ethylene transverse jets in supersonic crossflows", *J. Propuls. Power*, **31**(3), 773-788.
Chang, W.K., Park, G., Jin, Y., and Byun, J. (2016), "Shock impinging effect on ethylene flameholding", *J. Propuls. Power*, **32**(5), 1230-1239.
Chang, E.W.K., Yang, S., Park, G., and Choi, H. (2018), "Ethylene flame-holding in double ramp flows", *Aerosp. Sci. Technol.*, **80**, 413-423.
Kim, K., Park, G., and Jin, S. (2019), "Flameholding characteristics of ethylene-fueled model scramjet in shock tunnel", *Acta Astronaut.*, **161**, 446-464.
Kim, I., Lee, S., Park, G., and Lee, J.K. (2017), "Overview of flow diagnosis in a shock tunnel", *Int. J. Aeronaut. Space Sci.*, **18**(3), 425-435.
Park, G., Hruschka, R., Gai, S.L., and Neely, A.J. (2008), "Flow establishment behind blunt bodies at hypersonic speeds in a shock tunnel", Proc. SPIE 7126, *28th International Congress on High-Speed Imaging and Photonics,* 71260I.
Joshi, M.V., and Reddy, N.M. (1986), "Aerodynamic force measurements over missile configurations in IISc shock tunnel at M_∞=5.5", Exp. Fluid., **4**, 338-340.
Satheesh, K., and Jagadeesh, G. (2009), "Analysis of an internally mountable accelerometer balance system for use with non-isotropic models in shock tunnels", *Meas.*, **42**(6), 856–862.
Sahoo, N., Mahapatra, D.R., Jagadeesh, G., Gopalakrishnan, S., and Reddy, K.P.J. (2003), "An accelerometer balance system for measurement of aerodynamic force coefficients over blunt bodies in a hypersonic shock tunnel", *Meas. Sci. Technol.*, **14**(3), 260-272.
Sahoo, N., Mahapatra, D.R., Jagadeesh, G., Gopalakrishnan, S., and Reddy, K.P.J. (2007), "Design and analysis of a flat accelerometer-based force balance system for shock tunnel testing", *Meas.*, **40**(1), 93-106.
Joarder, R., and Jagadeesh, G. (2004), "A new free floating accelerometer balance system for force measurements in shock tunnels", *Shock Waves*, **13**(5), 409–412.
Mee, D.J. (2003), "Dynamic calibration of force balances for impulse hypersonic facilities", *Shock Waves*, **12**(6), 443–455.
Jo, S. M., Shim, H., Park, G., Kwon, O.J., and Kim, J. G. (2019), "Temperature determination in a shock tube using hydroxyl radical AX band emission", *Phys. Fluids,* **31**(2), 026109.
Yang, Y., Kim, I., and Park, G. (2019), "Experimental and numerical study of oxygen catalytic recombination of SiC-coated material", *Int. J. Heat. Mass Transf.*, **143**, 118510.
Kim, I., Park G., and Na J.J. (2019), "Experimental study of surface roughness effect on oxygen catalytic recombination", *Int. J. Heat. Mass Trans.*, **138**, 916-922.
Lee, S., Song, H., and Park, G. (2020), "Study of strut interference in high-speed flows", *Exp. Fluids*, **61**(4).
Prost, R., and Goutte, R. (1984), "Discrete constrained iterative deconvolution algorithms with optimized rate of convergence", *Signal Process.*, **7**(3), 209–230.